REPORT DOCUMENTATION PAGE

AFRL-SR-AR-TR-04-

0474

1. REPORT DATE (DD-MM-YYYY)	2. REPORT TYPE	3. DATES COVERED (From - To)
	Final Report	1 Jan 2002 - 30 Jun 2003

4. TITLE AND SUBTITLE
Energy Based Design and Control for Innovative Air Vehicle Concepts

5a. CONTRACT NUMBER

5b. GRANT NUMBER
F49620-02-1-0081

5c. PROGRAM ELEMENT NUMBER

6. AUTHOR(S)
Gregory Washington

5d. PROJECT NUMBER

5e. TASK NUMBER

5f. WORK UNIT NUMBER

7. PERFORMING ORGANIZATION NAME(S) AND ADDRESS(ES)
Ohio Stative University
206 West 18th Avenue
Columbus OH 43210-1107

8. PERFORMING ORGANIZATION REPORT NUMBER

9. SPONSORING/MONITORING AGENCY NAME(S) AND ADDRESS(ES)
USAF/AFRL
AFOSR
801 N. Randolph Street NA
Arlington VA 22203

10. SPONSOR/MONITOR'S ACRONYM(S)
AFOSR

11. SPONSOR/MONITOR'S REPORT NUMBER(S)

12. DISTRIBUTION/AVAILABILITY STATEMENT

Distribution Statement A. Approved for public release; distribution is unlimited.

20040921 046

13. SUPPLEMENTARY NOTES

14. ABSTRACT

In nature, birds change shape of their wings to achieve proper flight performance. In fact a falcon can glide or loiter at tremendous heights and then dive at three times its gliding speed to strike its prey. Falcons are able change the geometry of their wings by bending them at the shoulder, elbow and wrist. They can also affect the camber of the wing, and even articulate feathers at the wing tip to influence induced drag. Although a falcon can change many aspects of its wing geometry the most significant changes are the change of span, dihedral, surface area and twist. These factors directly affect stability and performance. Similarly an aircraft's wings are deformed significantly due to high aerodynamic pressure during flight maneuvers. A properly deformable aircraft structure is expected to enable the aircraft to have faster and gentler maneuver as well as more efficient and safer performance. Our goal as researchers is to learn from nature and to apply its principles in the next generation of morphing aircraft.

15. SUBJECT TERMS

16. SECURITY CLASSIFICATION OF:			17. LIMITATION OF ABSTRACT	18. NUMBER OF PAGES	19a. NAME OF RESPONSIBLE PERSON
a. REPORT	b. ABSTRACT	c. THIS PAGE			19b. TELEPHONE NUMBER (Include area code)
U	U	U	UU	14	

Energy Based Design and Control for Innovative Air Vehicle Concepts

Gregory Washington (washington.88@osu.edu)
Ohio State University
206 West 18th Ave
Columbus, OH 43210-1107
(614)-292-8486 (W)
(614)-292-3163 (F)

Final Report

In nature, birds change the shape of their wings to achieve proper flight performance. In fact a falcon can glide or loiter at tremendous heights and then dive at three times its gliding speed to strike its prey. Falcons are able change the geometry of their wings by bending them at the shoulder, elbow and wrist. They can also affect the camber of the wing, and even articulate feathers at the wing tip to influence induced drag. Although a falcon can change many aspects of its wing geometry the most significant changes are the change of span, dihedral, surface area and twist. These factors directly affect stability and performance. Similarly, an aircraft's wings are deformed significantly due to high aerodynamic pressure during flight maneuvers. A properly deformable aircraft structure is expected to enable the aircraft to have faster and gentler maneuver as well as more efficient and safer performance. Our goal as researchers is to learn from nature and to apply its principles in the next generation of morphing aircraft.

In recent years, the design and control of deformable aircraft structures has become an active topic of research in the aerospace community. Federal Research Laboratories such as Wright Laboratory, NASA Langley, and DARPA along with industrial collaborators such as Northrop Grumman, Boeing, and Lockheed Martin are actively engaged in research and development of this challenging multidisciplinary area (elastic structures, actuators, sensors, external aeroelasticity, flight mechanics, and control). Towards that end, several novel technologies, such as flow control and multifunctional structures, have emerged over the last decades that have the potential to revolutionize air vehicle concepts. The main issue is that virtually all of this work has been conducted at the component level with little to no attention being placed on scalable system integration, performance metrics, and system design and integration. ***The objective of this research was to develop a scalable design process that utilizes energy based metrics to identify candidate adaptive system concepts for the purpose of designing multi-mission vehicle concepts. An additional caveat of this research lied in the development of advanced sensors and actuator mechanization.*** Energy was chosen because it provided a medium where all concepts could be represented and judged in a consistent fashion. It is envisioned that the concepts outlined in this final report will provide a novel methodology for predicting the type, placement, and operation of actuators and sensors for air vehicles that incorporate large scale shape changing (or its effect). Potential new vehicles that can emerge from this technology include multi-mission vehicles such as combination strike-loiter or strike-surveillance vehicles.

As stated earlier the overall goal of this research was to develop a scalable design process that utilizes energy based metrics to identify candidate adaptive aircraft concepts for the purpose of designing multiple mission aircraft. The pedagogy for accomplishing this task is described in the following conceptual model:

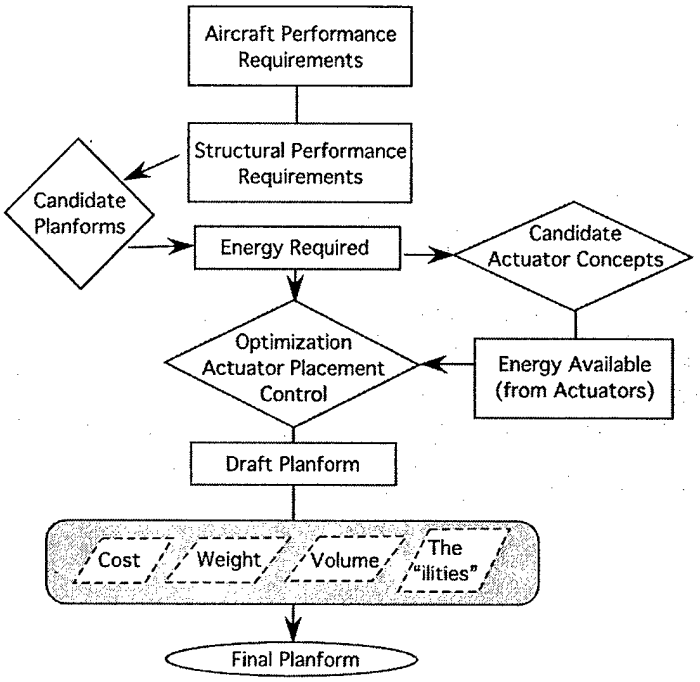

Figure 1. Energy Based Design Conceptual Model

Notice that the conceptual model is general enough to allow for competing designs (i.e. nozzle based flow control) to be compared with basic structural mechanics based designs. This is because at some level everything boils down to "Joules in and Joules out", thus energy is sort of a common denominator. In this construct the "customer" defines what the performance bounds of the aircraft should be. Aerodynamicists define what the structural performance requirements are. This may be wing shape, surface pressure distribution, etc. Sets of candidate planforms are then chosen and the candidate that requires the minimum amount of energy to achieve the proper shape is determined (detail in Task 1). Once a particular planform has been chosen, actuator systems that are capable of delivering the "energy" necessary are chosen. Here we use the term "energy" loosely, because energy here can mean energy density, volumetric energy density, etc (detail in Task 2). The idea is to eliminate actuator systems that cannot deliver the necessary planform or those that don't fit the geometrical or weight constraints. Optimization techniques will then be used to place the candidate actuator concepts optimally on the structure (detail in Task 3). This methodology makes use of novel concepts like simulated annealing and exergy analysis. In task 4 advanced sensor technology based on Polyvinylidene Fluoride (PVDF) was utilized. Instead of using strain gages, PVDF was used as a "pseudo" continuous stain measurement device. The main idea was to develop a measurement technique that converts strains to displacements.

Task 5 Involved an analytical investigation the behavior of a coupled, loaded actuator-mechanism system, which was the main element of a modern adaptive structure. The analysis is pursued from an energy transfer perspective. It coupled the actuator to a compliant mechanism and incorporated the interactions between this mechanized system and an applied load. Once the modeling, mechanization, and sensing techniques have been developed, controls will be employed to get the most out of the competing actuator concepts and it will also be used as a methodology for further reduction and integration (detail in Task 6). Note: the conceptual model has a layer where weight, volume, cost and the "ilities" (reliability, manufacturability, maintainability) can be considered directly. **The work in this proof of concept study makes significant progress in the first five task, the others are left for future proposed funding.** In order to accomplish the stated goals as explained by the conceptual model, this research is comprised of six distinct tasks that synergistically relate to the previously mentioned objectives.

Task 1. Development of an energy based methodology for aeroelastic structural deformations

An equivalent amount of energy needed to deform a structure can be calculated based on the specifications for a particular vehicle performance metric (e.g. roll) and the geometric and mechanical properties. This calculation can take into account the energy associated with phenomena involving interactions among inertial, aerodynamic, and elastic forces. Some of the metrics could be dynamic responses such as flutter, buffet, and transient loads or static phenomena such as, load distribution for minimizing drag, divergence, and control effectiveness. For this proof of concept research we will initially focus on static deformation phenomena. The performance metrics revolve around minimizing induced drag and maximizing the roll performance. These are key parameters that cover a large range of the flight profile. *Induced drag is a key parameter in air vehicles that are expected to have a long loiter and cruise flight segments, such as the Global Hawk, and roll performance is a key metric for any flight vehicle. For this reason we will focus on minimizing drag and improving roll performance.* If the method proves useful we will then proceed to address dynamic features such as flutter suppression.

Energy methods for describing the response of structural systems are well known and have been used for over half a century. The question that arises now is "can an energy based methodology be used to optimize key structural parameters and actuator locations". Energy may be an excellent metric since actuator performance is best described with these units. This will be discussed more in the next section.

In this research we have defined a framework that will allow for the incorporation of a distribution network of actuators to control structural deformation in the most efficient fashion. This may include deforming the entire wing or just key parts such as leading and trailing edges. With this in mind, it is recognized that the equations of motion for multidisciplinary aeroelastic systems can be seamlessly developed in 'generalized' coordinates instead of orthogonal modal coordinates. The main caveat of doing this lies in the fact that the elastic structure, actuator coupling, aerodynamic pressure distribution, and flight mechanics will be simultaneously considered in the direct 'generalized'

coordinates formulation. We have utilized this construct to model appropriate planforms. More general or field problems were modeled incorporating these concepts into a program that uses finite element analysis and incorporates various loadings. An example of the main interface and the output of the program is shown in figure 2. The dots on the figure to the right represent actuators.

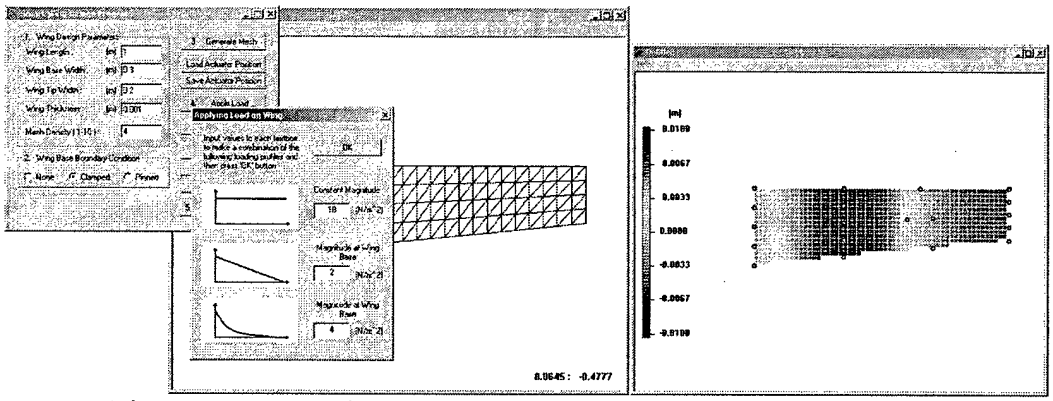

Figure 2. Smart Wing Analysis Program (SWAP): Main Interface

Task 2. Development of an Energy Based Methodology for classifying actuators

In task one the energy required to conduct a particular movement (or shape) was calculated. It was assumed that the required actuator is capable of producing the movement. The next step was to calculate the energy that a particular actuator is capable of producing. This step will clearly eliminate some concepts and will elevate others. Various actuator and sensor concepts can be examined here for feasibility (i.e. smart materials, conventional actuators and sensors, other systems avionics, etc.). Since the structural maneuvers given in task 1 are represented in an *energy-required* context the actuators in this section were classified by some form of energy production context. In order to achieve the deflections necessary for various maneuvers more than twenty different actuators were classified using the SWAP program outlined in task 1 (see table 1). Metrics like energy density and power density volumetric energy density, along with stroke and force were utilized because they represent entities that can be easily scaled. Remember the overall goal of this part of the study is the calculation of the maximum *actuator energy available* from a particular concept.

The specific output energy per unit mass	$U_e = \frac{Output\ Energy}{Mass\ Density} = \frac{\frac{1}{2} E_e \varepsilon^2}{\rho_e}$	2.1
The power conversion efficiency	$power\ efficiency(\eta) = \frac{output\ power(P_{out})}{input\ power(P_{in})}$ ex) $electrical\ power(P_{in}) = voltage \times current$	2.2

	$mechnical\ power(P_{out}) = force \times velocity$
The mechanical efficiency	$\eta_{mech} = \dfrac{Actuation\ output\ energy}{Active\ element\ energy}$ Ex.) Piezoelectric materials; $\eta_{mech(piezo)} = \dfrac{\frac{1}{2}K_a q^2}{\frac{1}{2}E_e \varepsilon^2 V_e}$ 2.3
Weight efficiency	$\eta_{mass} = \eta_{mech}\dfrac{Active\ element\ mass}{Total\ mass}$ 2.4

Task 3: Energy-based design optimization and sensitivity analysis

In this task, the mission requirements are defined as an energy problem. The optimization task involves the design of the actuators (type and location) for minimizing the waste energy. The original proposal (3 year proposal) stated that exergy would be used but since the research was only funded for one year (as highlighted in the updated statement of work) the initial energy analysis and optimization could only be completed. Besides, the given aerodynamic platform, the structure was designed so that it can maximize energy requirements using active controls in satisfying the flight performance requirements. In this particular task, issues addressed were the number and type of actuators, placement of actuators, placement of spars and ribs for the given planform, structural skin thickness, and the sizes of the stiffeners. The optimization problem was challenging in the sense it has integer variables (number of actuators, spars and ribs), discrete variables (type of actuators, location of spars and ribs) and continuous variables (skin thickness, spar and rib sizes, and location of the actuators). Hence, the optimization problem was solved using a combination of methods based on which type of sub-optimization problem is addressed. For actuator placement multiple techniques will be employed based on actuator controllability, simulated annealing, and univariate techniques. An overview of the research is given here for clarity. Assume the structure is described by the following differential equation

$$m\ddot{u}(x,t) + L(u(x,t)) = f(x,t) \tag{3.1}$$

Where we will define the stiffness operator as L, u(x,t) is the deformation, and f(x,t) is the external excitation. The associated eigenvalues are defined as λ_r and the eigenvectors are defined as $\phi_r(x)$. The modal equations can be written as

$$\ddot{q}_r(t) = -\omega_r^2 q_r(t) + Q_r(t) \tag{3.2}$$

where $q_r(t)$ are the modal displacements and $Q_r(t)$ are the modal forces which are related to $u(x,t)$ and $f(x,t)$ by the orthonormality conditions. The case of point actuators

can be incorporated into $Q_r(t)$ and then the modal equations can be converted into state space form.

We can now describe a new system by considering only the relevant modes

$$\ddot{y} + Ly = h \tag{3.3}$$

where

$$y = \begin{bmatrix} q_1 \\ \mathsf{M} \\ q_{n_r} \end{bmatrix}, \quad L = \begin{bmatrix} \omega_1^2 & & 0 \\ & \mathsf{O} & \\ 0 & & \omega_{n_r}^2 \end{bmatrix} \quad h = \begin{bmatrix} \sum_{i=1}^{n_a} \phi_1(x_i) f_i(t) \\ \mathsf{M} \\ \sum_{i=1}^{n_a} \phi_{n_r}(x_i) f_i(t) \end{bmatrix} \tag{3.4}$$

In state space form the system can be written as

$$\underbrace{\begin{bmatrix} \dot{y} \\ \ddot{y} \end{bmatrix}}_{\dot{x}} = \underbrace{\begin{bmatrix} 0 & I \\ -L & 0 \end{bmatrix}}_{A} \underbrace{\begin{bmatrix} y \\ \dot{y} \end{bmatrix}}_{x} + \underbrace{\begin{bmatrix} 0 & & 0 \\ \phi_1(x_1) & \Lambda & \phi_1(x_{n_a}) \\ \mathsf{M} & & \mathsf{M} \\ \phi_{n_r}(x_1) & \Lambda & \phi_{n_r}(x_{n_a}) \end{bmatrix}}_{B} \underbrace{\begin{bmatrix} f_1(t) \\ \mathsf{M} \\ f_{n_a}(t) \end{bmatrix}}_{u} \rightarrow \dot{x} = Ax + Bu \tag{3.5}$$

The controllability matrix is given by

$$C = \begin{bmatrix} B & AB & \mathsf{L} & A^{2n_r-1}B \end{bmatrix} \tag{3.6}$$

The controllability matrix measures how controllable a system is. The larger the value of the determinant of the C matrix, the more controllable the system is. The more controllable a system, the smaller amount of **energy** is needed to force the system to the reference state. If the determinant of the C matrix is zero then the system is uncontrollable and even with an infinite amount of energy you cannot reach the reference shape. We need to calculate the relative "size" of the C matrix. This can be accomplished by using Singular Value Decomposition (SVD). NOTE: The dimension of the controllability matrix is $2n_r \times 2n_r n_a$.

For SVD Let

$$G = \det\left(CC^T\right) = \prod_{i=1}^{2n_r} \sigma_i^2 \tag{3.7}$$

where the $\sigma's$ are the singular values. Notice that as various actuator positions are varied the value of G will change. The maximum value of G is associated with the optimum positions of the actuators. We find the maximum values by using differential calculus. In fact, we take the **derivative (Gradient)** and set it equal to zero to find the locations of

all possible critical points. The critical points are those values where the positions can cause a maximum or minimum. To determine whether the values are actually minimums or maximums the **second derivative (Jacobian)** is used.

The sensitivity of the planform selected is an important activity in this project. For conducting the preliminary design, the appropriate planform dimensions have to be selected to meet both the roll maneuverability and the cruise condition of the flexible vehicle. Multi-objective missions need the sensitivities of the span and chord lengths, aspect ratio, sweep, number of wing box cells, etc. The strain energy, power conversion efficiency, and exergy are the quantities studied based on the computer modeling of integrated structure, aerodynamics and active control systems. These sensitivities enable 'what-if' parametric studies and provide the design trends for compromising the vehicle missions between the dash and loiter and their associated energy requirements. Direct Search, Simulated Annealing, Genetic algorithms, and response surface methods are also potential optimization candidates. An example of the optimization interface is shown in figure 3.

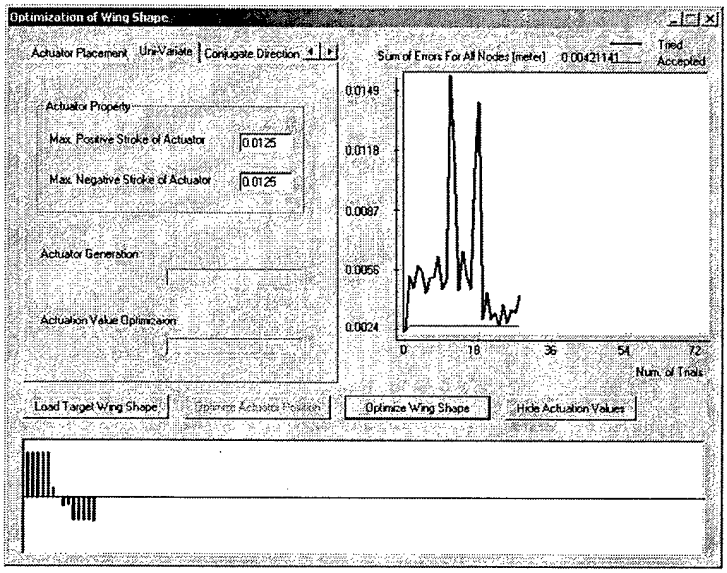

Figure 3. Optimization Interface

Task 4. Advanced Sensor Development

Since the structure deforms by strains one has to be able to relate these strains to the actuator displacements given in the previous section. In this section a derivation is presented that relates strain to displacement in the structure. Specifically, the structure will be partitioned into two elements and the displacements from each element will be related to the global displacement of the structure. The two individual beam elements and the assembled beam are shown in Figure 4.1 with individual coordinate systems and the displacement and slope at each node labeled.

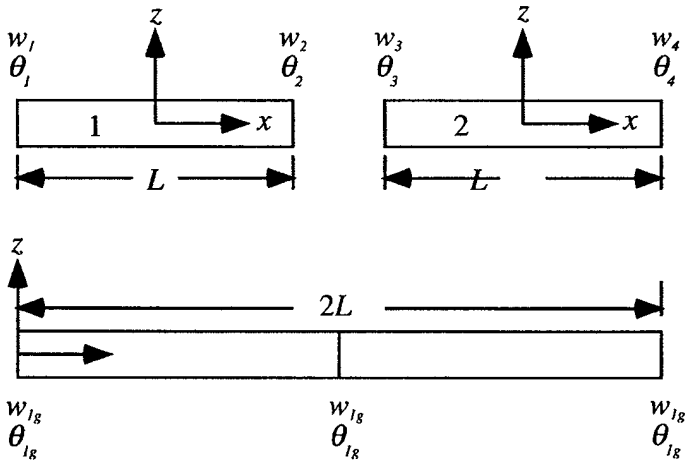

Figure 4.1: Individual beam elements and their relation to the assembled beam.

4.1 Derivation of Strain-to-Displacement Relation

The equation that relates strain to displacement is

$$\mathbf{S} = \mathbf{M}^T \delta, \tag{4.1}$$

where S, M^T, δ are the strain vector, strain-to-displacement matrix, and displacement vector respectively. The values of S will be measured and δ will be calculated based on the measured values. Therefore it is necessary to first determine the values of M^T, and this is accomplished by first examining the equation of motion. The equation of motion for an unloaded beam is given by the following spatial equation

$$\frac{\partial^4 \phi(x)}{\partial x^4} = 0. \tag{4.2}$$

The following solution will be assumed for Equation (4.2)

$$\phi(x) = a_1 + a_2 x + a_3 x^2 + a_4 x^3. \tag{4.3}$$

Taking the first derivative of Equation (4.3) with respect to x gives the following expression

$$\theta(x) = \frac{\mathrm{d}\phi(x)}{\mathrm{dx}} = a_2 + 2a_3 x + 3a_4 x^2, \tag{4.4}$$

which is an equation for the slope of the beam.

At the boundaries of the element there will be some displacement and some slope and is represented mathematically as

$$\phi\left(\frac{-L}{2}\right) = w_1 \tag{4.5}$$

$$\theta\left(\frac{-L}{2}\right) = \theta_1 \tag{4.6}$$

$$\phi\left(\frac{L}{2}\right) = w_2 \tag{4.7}$$

$$\theta\left(\frac{L}{2}\right) = \theta_2, \tag{4.8}$$

where L is the length of an individual beam element. Combining Equation (4.3) and (4.4) with Equations (4.5) – (4.8) yields

$$\begin{bmatrix} w_1 \\ \theta_2 \\ w_2 \\ \theta_2 \end{bmatrix} = \begin{bmatrix} 1 & -\frac{L}{2} & \frac{L^2}{4} & -\frac{L^3}{8} \\ 0 & 1 & -L & \frac{3L^2}{4} \\ 1 & \frac{L}{2} & \frac{L^2}{4} & \frac{L^3}{8} \\ 0 & 1 & L & \frac{3L^2}{4} \end{bmatrix} \begin{bmatrix} a_1 \\ a_2 \\ a_3 \\ a_4 \end{bmatrix}. \tag{4.9}$$

Solving Equation (4.9) for a_i leads to

$$\begin{bmatrix} a_1 \\ a_2 \\ a_3 \\ a_4 \end{bmatrix} = \begin{bmatrix} \frac{1}{2} & \frac{L}{8} & \frac{1}{2} & -\frac{L}{8} \\ \frac{3}{2L} & -\frac{1}{4} & \frac{3}{2L} & -\frac{1}{4} \\ 0 & -\frac{1}{2L} & 0 & \frac{1}{2L} \\ \frac{2}{L^3} & \frac{1}{L^3} & -\frac{2}{L^3} & -\frac{1}{L^2} \end{bmatrix} \begin{bmatrix} w_1 \\ \theta_2 \\ w_2 \\ \theta_2 \end{bmatrix}. \tag{4.10}$$

The strain of the beam element can be written as

$$S(x) = \frac{\mathrm{d}^2\phi(x)}{\mathrm{d}x^2} = 2a_3 + 6a_4 x. \tag{4.11}$$

Substituting the values of a3 and a4 from Equation (4.10) into Equation (4.11) yields

$$S(x) = -\frac{1}{L}\theta_1 + \frac{1}{L}\theta_2 + \left(\frac{12}{L^3}w_1 + \frac{6}{L^2}\theta_1 - \frac{12}{L^3}w_2 + \frac{6}{L^2}\theta_2\right)x. \tag{4.12}$$

Equation (4.12) will now be evaluated at the two Barlow points, given by x = ±

$$\mathbf{S} = \begin{bmatrix} S\left(-\frac{L}{2\sqrt{3}}\right) \\ S\left(\frac{L}{2\sqrt{3}}\right) \end{bmatrix} = \frac{1}{L^2}\begin{bmatrix} -2\sqrt{3} & -\left(1+\sqrt{3}\right)L & 2\sqrt{3} & \left(1-\sqrt{3}\right)L \\ 2\sqrt{3} & \left(-1+\sqrt{3}\right)L & -2\sqrt{3} & \left(1+\sqrt{3}\right)L \end{bmatrix}\delta, \tag{4.13}$$

where

$$\delta = \begin{bmatrix} w_1 \\ \theta_1 \\ w_2 \\ \theta_2 \end{bmatrix}. \tag{4.14}$$

Comparing Equation (4.13) to Equation (4.1), the following relation can be seen

$$\mathbf{M}^T = \frac{1}{L^2}\begin{bmatrix} -2\sqrt{3} & -\left(1+\sqrt{3}\right)L & 2\sqrt{3} & \left(1-\sqrt{3}\right)L \\ 2\sqrt{3} & \left(-1+\sqrt{3}\right)L & -2\sqrt{3} & \left(1+\sqrt{3}\right)L \end{bmatrix}. \tag{4.15}$$

Equations (4.15) and (4.1) give a relation between strain and displacement for one element. The individual beam elements must now be related to the global system. This is accomplished by creating a Boolean matrix that relates the local beam elements to the global structure as follows [28]

$$\delta_l = \mathbf{B}\delta_g, \tag{4.16}$$

where δ_l is a vector of the local or partitioned displacements, δ_g is a vector of the global

or assembled displacements, and B is the partitioning operator, which relates the two displacement vectors. For a two-element beam with free-free boundary conditions, Equation (4.16) becomes

$$\begin{bmatrix} w_1 \\ \theta_1 \\ w_2 \\ \theta_2 \\ w_3 \\ \theta_3 \\ w_4 \\ \theta_4 \end{bmatrix} = \begin{bmatrix} 1 & 0 & 0 & 0 & 0 & 0 \\ 0 & 1 & 0 & 0 & 0 & 0 \\ 0 & 0 & 1 & 0 & 0 & 0 \\ 0 & 0 & 0 & 1 & 0 & 0 \\ 0 & 0 & 1 & 0 & 0 & 0 \\ 0 & 0 & 0 & 1 & 0 & 0 \\ 0 & 0 & 0 & 0 & 1 & 0 \\ 0 & 0 & 0 & 0 & 0 & 1 \end{bmatrix} \begin{bmatrix} w_{1g} \\ \theta_{1g} \\ w_{2g} \\ \theta_{2g} \\ w_{3g} \\ \theta_{3g} \end{bmatrix}. \tag{4.17}$$

For a beam with clamped-free boundary conditions the displacement and slope at the clamped edge will be zero in both the local and global elements and is expressed mathematically as

$$w_1 = 0 \tag{4.18}$$

$$\theta_1 = 0 \tag{4.19}$$

$$w_{1g} = 0 \tag{4.20}$$

$$\theta_{1g} = 0. \tag{4.21}$$

Applying Equations (4.18) – (4.21) to Equation (4.17) eliminates the first two elements of the displacement vectors and the first two columns and rows of the B matrix. Rewriting Equation (4.17) yields,

$$\begin{bmatrix} w_2 \\ \theta_2 \\ w_3 \\ \theta_3 \\ w_4 \\ \theta_4 \end{bmatrix} = \begin{bmatrix} 1 & 0 & 0 & 0 \\ 0 & 1 & 0 & 0 \\ 1 & 0 & 0 & 0 \\ 0 & 1 & 0 & 0 \\ 0 & 0 & 1 & 0 \\ 0 & 0 & 0 & 1 \end{bmatrix} \begin{bmatrix} w_{2g} \\ \theta_{2g} \\ w_{3g} \\ \theta_{3g} \end{bmatrix}. \tag{4.22}$$

The strain-displacement relation matrix MT must be modified to incorporate two beam elements and the clamped boundary condition, thus creating a new matrix, M_g^T, defined as

$$\mathbf{M}_g^T = \frac{1}{L^2} \begin{bmatrix} 2\sqrt{3} & \left(1-\sqrt{3}\right)L & 0 & 0 & 0 & 0 \\ -2\sqrt{3} & \left(1+\sqrt{3}\right)L & 0 & 0 & 0 & 0 \\ 0 & 0 & -2\sqrt{3} & -\left(1+\sqrt{3}\right)L & 2\sqrt{3} & \left(1-\sqrt{3}\right)L \\ 0 & 0 & 2\sqrt{3} & \left(-1+\sqrt{3}\right)L & -2\sqrt{3} & \left(1+\sqrt{3}\right)L \end{bmatrix}, \tag{4.23}$$

which is just a block diagonal matrix formed form M^T with the first two column removed to account for the clamped boundary condition. Now, Equation (4.1) can be rewritten to obtain a relationship between strain and the global displacements by substituting Equation (4.16) for δ_g and Equation (4.23) for M^T, which results in

$$\mathbf{S} = \mathbf{M}_g^T \mathbf{B} \delta_g, \tag{4.24}$$

where B takes on the value given in Equation (4.22). Note that $M_g^T \mathrm{B}$ forms a square matrix that is non-singular and can therefore be inverted to solve for δ_g

$$\delta_g = \left[\mathbf{M}_g^T \mathbf{B}\right]^{-1} \mathbf{S}, \tag{4.25}$$

where

$$\left[\mathbf{M}_g^T \mathbf{B}\right]^{-1} = \begin{bmatrix} \frac{\sqrt{3}}{12}\left(1+\sqrt{3}\right)L^2 & \frac{\sqrt{3}}{12}\left(-1+\sqrt{3}\right)L^2 & 0 & 0 \\ \frac{1}{2}L & \frac{1}{2}L & 0 & 0 \\ \frac{1}{12}\left(9+\sqrt{3}\right)L^2 & -\frac{1}{12}\left(-9+\sqrt{3}\right)L^2 & \frac{\sqrt{3}}{12}\left(1+\sqrt{3}\right)L^2 & \frac{\sqrt{3}}{12}\left(-1+\sqrt{3}\right)L^2 \\ \frac{1}{2}L & \frac{1}{2}L & \frac{1}{2}L & \frac{1}{2}L \end{bmatrix}. \tag{4.26}$$

The global displacements have been solved at the edges of each element, and now the displacements at any point x along the length of the beam can be solved. The global displacements are related to the local displacements through the Boolean matrix B as shown in Equation (4.22) and therefore the (a) coefficients from the assumed solution can be solved using Equation (4.10) which are then combined with Equation (4.3) to obtain the spatial solution. This must be done individually for each element over the range $-\frac{L}{2} \le x \le \frac{L}{2}$ which is the local coordinate system of each element. The results must then be relocated based on the global coordinate system, therefore the spatial solution from the first element is moved to the range 0 -> x -> L and the spatial solution for the second element is moved to the range L -> x -> 2L.

4.2 Experimental Strain-Displacement Results

The equations presented in Section 4.1 will now be tested experimentally. The experimental setup is shown in Figure 4.2 and consists of a beam with four piezoelectric strain sensors mounted at specific points and a shaker that excites the beam. The beam is aluminum with thickness of 0.0625 inches, height of 2 inches, and the length is 10 inches. Therefore, the length of an individual beam element, L, is 5 inches. The first two natural frequencies of the beam were determined to be at 19Hz and 119Hz and results will be shown for tests run at both frequencies. Each piezoelectric strain sensor has a length of 0.5 inches and height of 0.25 inches and are centered at the Barlow (Gauss) points of each element listed in Equation (4.14). On the global coordinate system, the sensors should be placed at the following x coordinate values: 1.0566, 3.9434, 6.0566, and 8.9434 inches, and the actual locations are close to these values, but the accuracy has practical limitations. The output form each sensor was connected to Siglab and sampled at 512Hz. The strain sensors are labeled S1, S2, S3, and S4 respectively moving from the clamped edge to the free edge.

The voltage output from each sensor for mode one vibration is shown in Figure 4.3. The relative magnitudes from each sensor can be compared to the expected results based on the curvature shown in Figure 4.4, and it can be seen that they both agree with

the following relations: S1 > S2 > S3 > S4. The displacement of the beam is shown in Figure 4.4, where the line represents the assumed solution that has been solved and the global displacements from Equation (4.26) are represented with a circle. The shape of Figure 4.4 can be compared to the mode 1 predicted shape and it can be seen that the two are in good agreement.

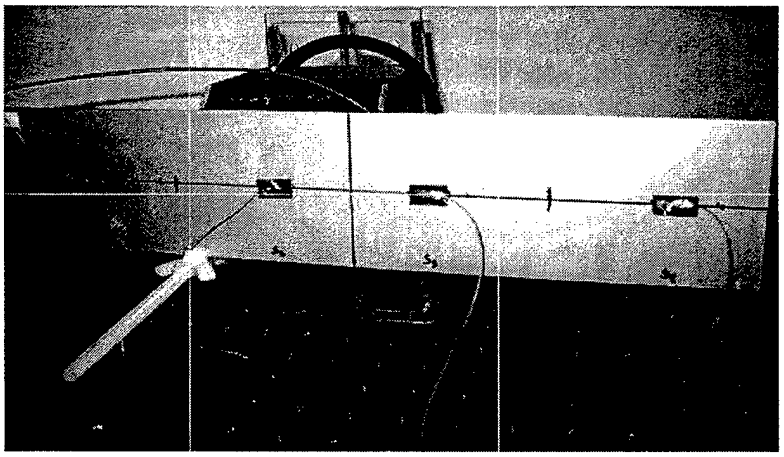

Figure 4.2: Experimental setup for testing the strain-to-displacement relationship equations.

Similarly, the voltage output from each sensor for mode two vibration is shown in Figure 4.5 and the corresponding displacement is shown in Figure 4.6. One can see clearly that the mode shape represents mode 2 of a cantilevered beam.

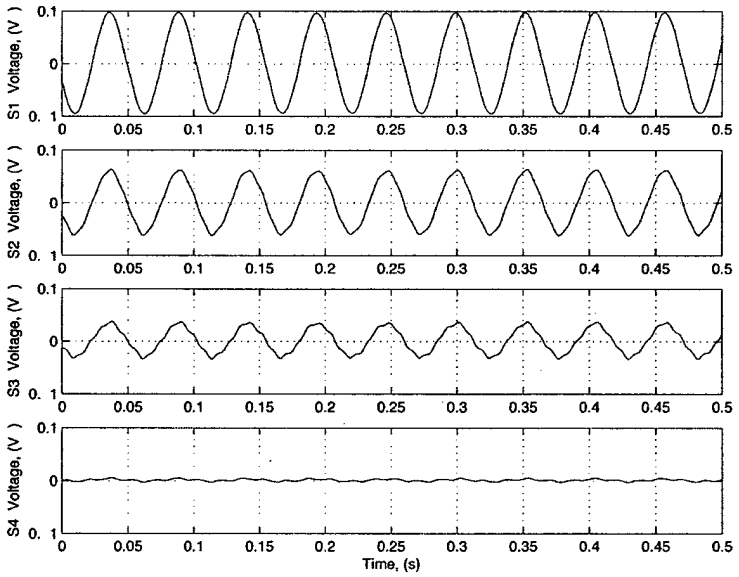

Figure 4.3: Voltage output from each piezoelectric strain sensor due to mode 1 vibration.

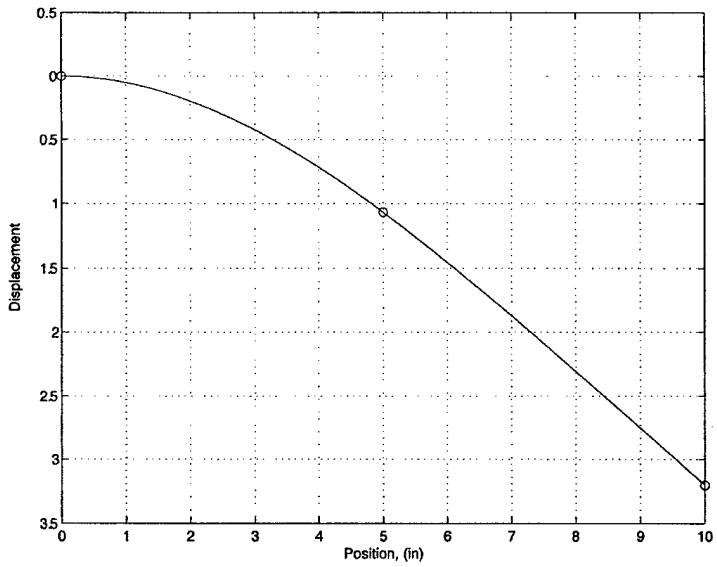

Figure 4.4: Displacement of the beam due to mode 1 vibration.

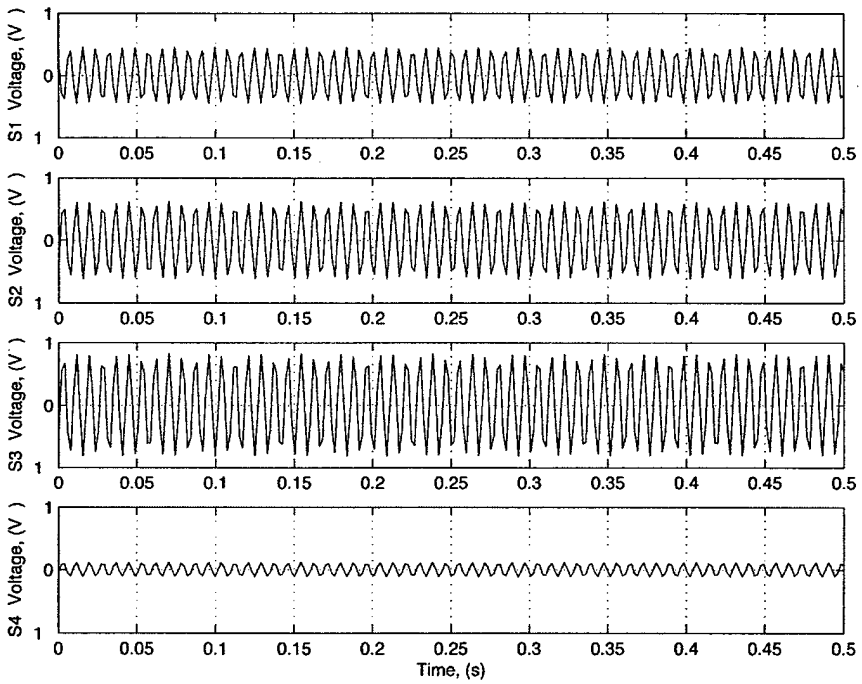

Figure 4.5: Voltage output from each piezoelectric strain sensor due to mode 2 vibration.

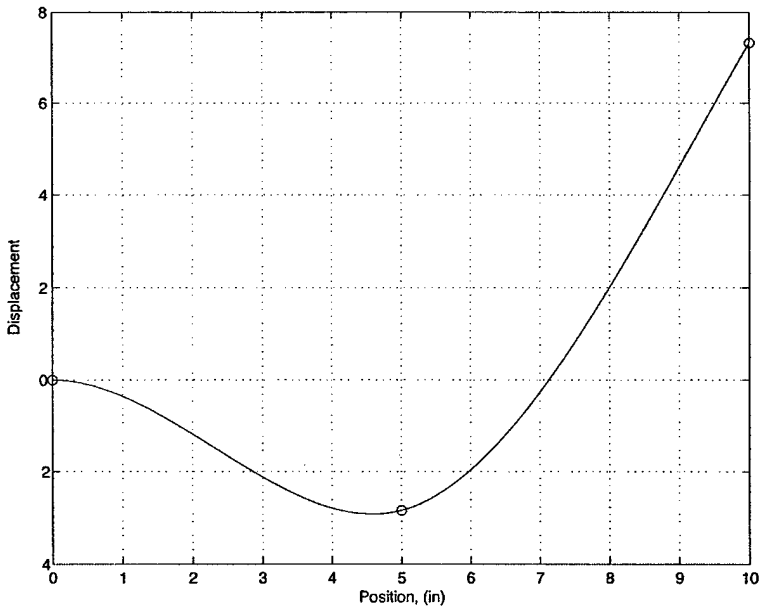

Figure 4.6: Displacement of the beam due to mode 2 vibration

There are a number of unresolved issues with the technique. While we get good results on the mode shape, the actual magnitudes are hard to calculate because of the complex impedances of most data acquisition systems. We are presently investigating modal observers to get a final answer.

Graduate Students

Bruce Isler, MS 2001, Thesis: Uniform Damping Node Control Theory Utilizing Shaped Piezoelectric Film

Fukashi Andoh, Ph.D. 2001, "Control of Distributed Parameter Systems using Piezoelectric Transducers, Post Doctoral researcher at OSU in the Vibration and Dynamics Laboratory. (w. Vadim Utkin)

Manuscripts

Andoh, F., Washington, G.N., V. Utkin "Shape Control of Distributed Parameter Reflectors Using Sliding Mode Control" *Proc. SPIE Int. Conference on Smart Structures and Materials*, 2001

Isler, B., and Washington, G.N., "Spatial Aperture Shading Applied to Distributed Systems for Uniform Damping Control", *Proc. SPIE Int. Conference on Smart Structures and Materials*, 2001, Vol. 4326, No. 61, pp. 548-558.

Andoh, F., Washington, G.N., and Utkin, V.,, "Efficient Shape Control of Distributed Reflectors with Discrete Piezoelectric Actuators", *Journal of Intelligent Material Systems and Structures,* **15**, No. 1., January 2004, pp. 3-15.